Ultra-Wide Band Polarization Converter Based on Ultra-Thin Bi-Layer Slot Structures

Jun-Ho Jeong, Jae-Yeong Lee, *Member, IEEE*, and Jae-Hyung Jang, *Senior Member, IEEE*

***Abstract*— An ultrathin linear-to-linear polarization converter exhibiting a high polarization conversion ratio (PCR) in an ultrawide bandwidth is fabricated on a printed circuit board (PCB). It is based on a bilayer slot structure that is electrically connected by via holes. Front- and back-sided slot structures are arranged in mutually orthogonal directions and function as receivers and radiators, respectively. The via holes provide a route for the transfer of electromagnetic energy received by the front-sided slot structures to the back-sided slot structures and radiate an electromagnetic wave having polarization orthogonal to that of the input electromagnetic wave. Moreover, two slots are employed for each unit cell design, and the locations of the via holes are carefully determined to achieve broadband polarization conversion. The via-hole positions that change the surface current distribution around the slot apertures enable the control of multiple resonance frequencies. Via holes are positioned to make first and second resonance frequencies that are blue-shifted toward the third resonance frequency, which broadens the operational band of the perfect polarization conversion. The 0.8 mm thick polarization converter exhibits PCR greater than 99% in the frequency band from 24.5 to 47 GHz.**

***Index Terms*— Frequency selective surface (FSS), polarization converter, slot structure, ultrawideband radiation, via hole.**

I. Introduction

POLARIZATION converters are often employed in microwave relaying systems to change the polarization of electromagnetic waves [1], [2], [3], [4], [5], [6], [7]. A linear-to-linear polarization converter rotates the polarization of a linearly polarized wave to form an orthogonal one. Conventional polarization conversion methods employ anisotropic materials that have different permittivities along the orthogonal optical axis [8], [9].

2-D frequency selective surfaces (FSSs) have received great attention due to their ability to manipulate the properties of electromagnetic waves. They have also been utilized for polarization conversion devices to overcome the drawback of conventionally bulky optical crystal-based polarization rotators. Polarization conversion has been achieved using the chirality of metamaterials [10], [11], [12], [13], [14] (i.e., the optical activity of chiral structures), but they exhibit high insertion loss and a small polarization rotation angle. To improve performance, the use of multilayer metamaterials has been proposed [15], [16], [17]. They achieved a polarization rotation angle of approximately 90° and broadband characteristics, but they have the disadvantage of a complex fabrication process.

Reflection- and transmission-type polarization converters have been studied for their high polarization conversion ratio (PCR) in the broad frequency band [15], [18], [19], [20], [21], [22], [23], [24], [25], [26]. Periodically arranged anisotropic metallic structures above a metallic plane have been used to expand their bandwidth. However, they exhibit a limited PCR of 80%–85% in the middle of the band and narrow bandwidth because the resonance frequencies are far apart. To overcome the limited PCR in the midband for radar-cross section (RCS) reduction applications, FSSs consisting of two dielectric layers and coded metasurface featuring PCR higher than 90% have been recently demonstrated in an ultrawide frequency band [27], [28], [29]. However, it is still challenging to realize ultrathin lightweight linear polarization conversion devices exhibiting PCR higher than 99% in ultrawide bandwidth [5], [30], [31], [32].

This article demonstrates an ultrathin transmission-type polarization converter that operates in the ultrawide frequency band from 24.5 to 47 GHz. The polarization converter was realized on a printed circuit board (PCB). The front and back metal layers of the PCB were utilized to fabricate bilayer FSSs connected through via holes. By using multiple slot apertures and via holes in a unit cell design, PCR higher than 99% and the fractional bandwidth of 62.9% were achieved on an ultrathin substrate.

II. Unit Cell Design and Simulation

The polarization converter was realized on PCB by using bilayer slot structures connected by 0.8 mm long via holes,

Manuscript received 26 October 2021; revised 5 July 2022; accepted 14 September 2022. Date of publication 27 October 2022; date of current version 19 January 2023. This work was supported in part by the Creative Materials Discovery Program through the National Research Foundation (NRF) funded by the Ministry of Education and the Ministry of Science and ICT under Grant 2017M3D1A1040834; in part by the KENTECH Research Grant under Grant KRG2021-01-011; and in part by the Korea Institute of Energy Technology Evaluation and Planning (KETEP) funded by the Ministry of Trade, Industry and Energy (MOTIE), Korea Government, under Grant 20224000000100 (GAMS). *(Corresponding author: Jae-Hyung Jang.)*

Jun-Ho Jeong was with the School of Electrical Engineering and Computer Science, Gwangju Institute of Science and Technology, Gwangju 61005, South Korea. He is now with Samsung Electronics, Pyeongtaek-si 17786, South Korea (e-mail: wjdjdwg@gmail.com)

Jae-Yeong Lee was with the Department of Nanobio Materials and Electronics, Gwangju Institute of Science and Technology, Gwangju 61005, South Korea. He is now with the Terahertz Research Section, Electronics and Telecommunications Research Institute (ETRI), Daejeon 34129, South Korea (e-mail: jylee82@gm.gist.ac.kr).

Jae-Hyung Jang is with the Department of Energy Engineering, Intelligent Electrical Safety, Power Semiconductor Concentration, KENTECH Institute of Energy Materials and Devices, Korea Institute of Energy Technology (KENTECH), Naju 58330, South Korea (e-mail: jjang@kentech.ac.kr).

Color versions of one or more figures in this article are available at https://doi.org/10.1109/TAP.2022.3216467.

Digital Object Identifier 10.1109/TAP.2022.3216467

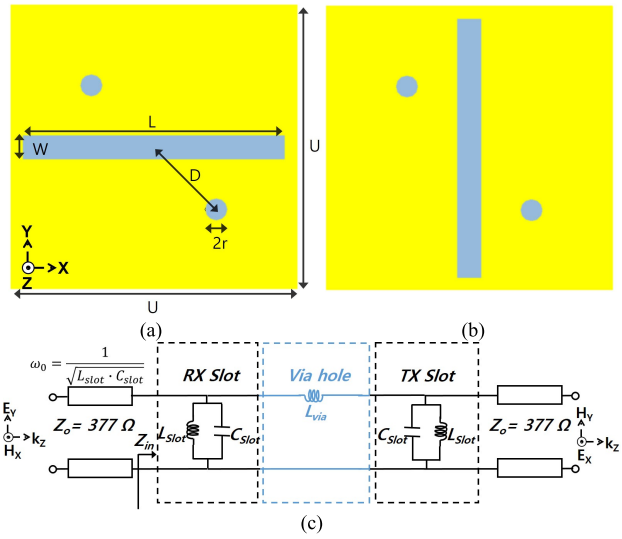

Fig. 1. Schematic design of the unit cell in the polarization converter and its equivalent circuit. (a) Front side and (b) back side. L = 4.2 mm, W = 0.4 mm, D = 1.4 mm, r = 0.2 mm, U = 4.6 mm, and the substrate thickness (T_S) = 0.8 mm. (c) Simplified equivalent circuit model of the polarization converter.

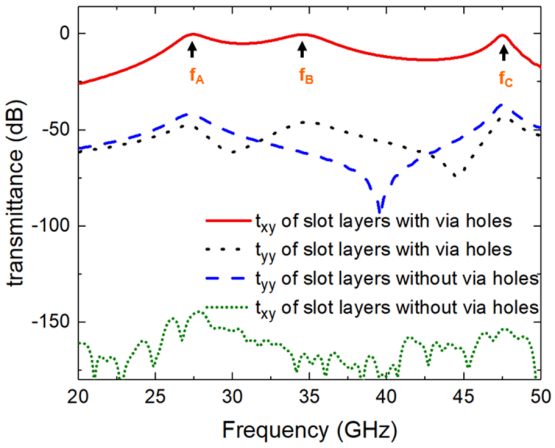

Fig. 2. Transmittance characteristics of slot structures with and without via holes.

as shown in Fig. 1(a) and (b). A unit cell consists of a front-side slot and a 90°-rotated back-side slot, connected by two via holes. The via-hole length is the same as the thickness (T_s = 0.8 mm) of the TLX-9 substrate. The diameter of the via holes is kept as small as possible (within the limit of the fabrication process) to minimize co-polarized transmission through the holes.

The operating principle of the proposed polarization converter can be understood by using the equivalent circuit shown in Fig. 1(c). The slot structures were represented by the parallel *LC* resonant circuits. The electrically short via hole can be regarded as a simple series-connected inductor, as depicted in Fig. 1(c). At resonance frequency, the parallel *LC* circuit is effectively open-circuited and the incident wave is resonantly transferred to the other parallel *LC* circuit representing the back-side slot structures via the series-connected inductor. By using the analysis method described in [30], the values of the inductance (L_{slot}) and capacitance (C_{slot}) of the slot structure in the unit cell were extracted and found to be 0.42 nH and 0.08 pF, respectively. The front of the polarization converter receives the incident electromagnetic wave at resonance frequencies and the back radiates the electromagnetic wave, as the front- and back-side slot structures act as a receiver and a transmitter, respectively, at the same resonance frequency. The slots are designed to be identical except in orientation. The via holes provide a route for the transfer of electromagnetic energy received by the front-side slot structures to the back-side slot structures and radiate an electromagnetic wave having polarization orthogonal to that of the input electromagnetic wave. The via holes also induce coupling between two resonant slot structures and resonance frequency split [33].

In the full-wave simulation using CST studio suite, transmission coefficients were obtained from a unit cell by applying a periodic boundary condition. The incoming electromagnetic wave propagates along the *z*-direction, and its polarization is kept along the *y*-axis. When the *y*-polarized plane wave is incident to the polarization converter, a resonating surface current is generated around the front-side slot aperture. Then, the surface current flows along the via holes, and a surface current is generated around the slot apertures on the back-side metal plane. The surface current around the slot apertures on the back side radiates an electromagnetic wave with 90°-rotated *x*-polarization [24]. Fig. 2 illustrates the co-polarized transmittance (t_{yy}) and cross-polarized transmittance (t_{xy}) of the slot structures with and without via holes. t_{xy} of the slot structures with via holes exhibits the bandpass characteristics at the three resonance peaks at f_A (27.5 GHz), f_B (34.5 GHz), and f_C (47.5 GHz). When the transmittance characteristics of two-sided slot structures with and without the via holes in Fig. 2 are compared, the via holes dramatically improve the transmittance characteristics. Even though the two-sided orthogonal slot structures without via holes exhibit very small t_{yy} value (<-50 dB level), t_{yy} exhibits two resonances at 27.3 and 47.6 GHz. The two resonance frequencies are essentially the same as f_A and f_C observed in t_{xy} and t_{yy} of the polarization converter with via holes. Therefore, it can be concluded that the transmittance peaks at f_A and f_C are due to the resonance of the slot structures. Considering the surface current distributions in Fig. 3(a) and (c) that show one minimum at f_A and two minima at f_C at each side of the slot structure, the transmittance peaks at f_A and f_C are due to the fundamental resonance and the second harmonic resonance of the slot structure, respectively.

The additional resonance at f_B is due to the presence of the via holes and is related to the location of the via holes as well as the slot length. By taking advantage of the additional resonance at f_B, a broad frequency band can be achieved by combining three frequency bands. In detail, when the center-to-center distance (D) between the slot and the via hole in Fig. 1 is 1.4 mm, the inductance of the via hole is obtained to be 1.2 nH by comparing circuit and simulation results. In the following, three methods are introduced to broaden the bandwidth using the location of via holes, double slot structures, and additional via holes.

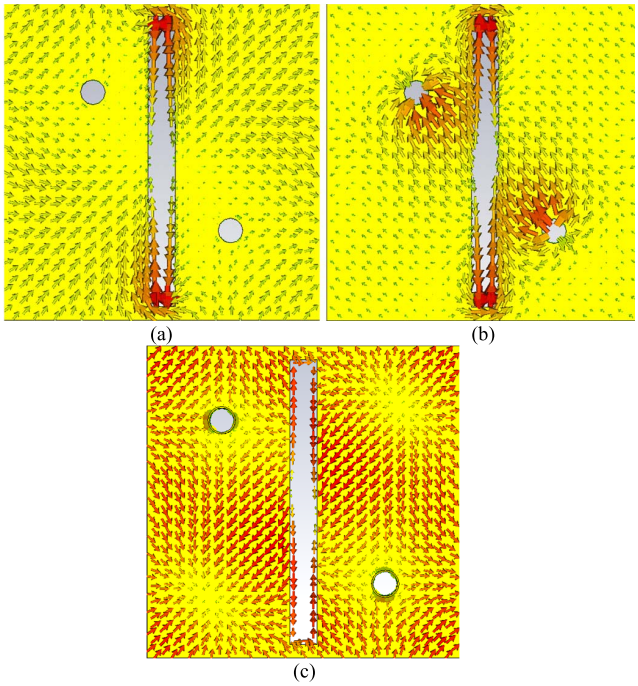

Fig. 3. Surface current distribution on the back side of polarization converter at resonance frequencies of (a) f_A (27.5 GHz), (b) f_B (34.5 GHz), and (c) f_C (47.5 GHz).

A. Diagonal Arrangement of via Hole

To understand the origin of the additional transmission peak corresponding to the resonance at f_B, the distribution of the surface charge induced on the polarization converter was analyzed.

In Fig. 4, the surface charge distributions that are extracted from the normal component of the time varying electric field on the front- and back-sides at the resonance frequencies of f_A, f_B, and f_C are compared. The red contour line shows a positive charge distribution, and the blue contour line shows a negative charge distribution. When a single-sided slot structure without via holes is considered, opposite surface charges are mostly distributed at the central part of the slot structure at the fundamental resonance frequency. However, the surface charge distribution of a polarization converter that employs the via holes is changed.

As shown in Fig. 4, the surface charges are concentrated on the first and third quadrants at the resonance frequency, f_A, and they are concentrated on the second and fourth quadrants at the additional resonance frequency, f_B. At the resonance frequency, f_A, time-varying opposite charge distributions make a time-varying surface current around the slot aperture and on the metal surface, as shown in Fig. 3(a). There is incoming current from some adjacent unit cells and outgoing current toward other adjacent unit cells, which suggests that the interaction between the neighboring unit cells also influences the surface current distribution on the metal plane. Because the radiated field of a magnetic moment is affected by the electric current flowing on the metal surface, as well as by the slot aperture size [25], the resonance frequencies of f_A and f_C are determined by the slot aperture length and unit cell size. This indicates that the surface current toward neighboring

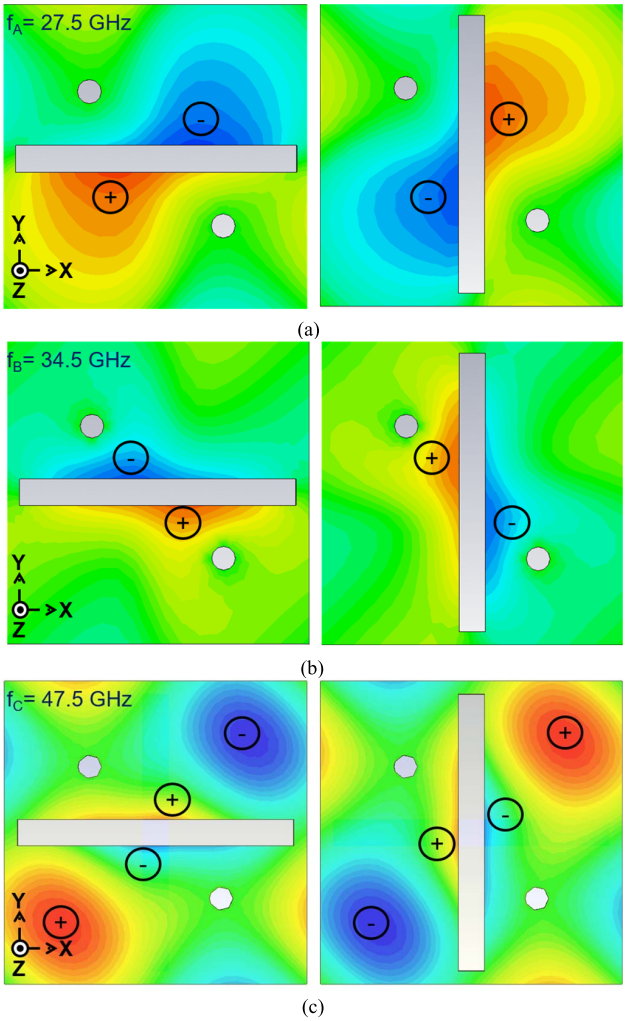

Fig. 4. Surface charge distributions of polarization converter on front side (left) and back side (right) at the resonance frequency of (a) f_A (27.5 GHz), (b) f_B (34.5 GHz), and (c) f_C (47.5 GHz).

unit cells, as well as the surface current around the slots, affects the field radiated at the resonance frequencies f_A and f_C. At the resonance frequency f_B, the charges formed around the via holes on the front and back sides have opposite polarity, as depicted in Fig. 4(b). This enhances the vertical current flow through the via holes, as illustrated in Fig. 3(b). The current density through the via holes at f_B is much higher than that at f_A and f_C. The surface current path length on the metal surface at f_A is determined by the unit cell length. On the other hand, the current path length through the via holes is shorter than the unit cell length, considering the very thin substrate. Thus, the additional resonance frequency f_B is higher than the fundamental slot resonance frequency, f_A. Because the resonating current through the via holes is very low at the frequencies of f_A and f_C, these resonance frequencies are not affected by the position of the via holes.

Considering the charge and surface current distributions, the resonance frequency, f_B, can be controlled by the positions of the via holes. As shown in Fig. 5, the changes in the positions of the via holes affect only f_B. By adjusting the location of the via holes, the resonance frequency, f_B, can

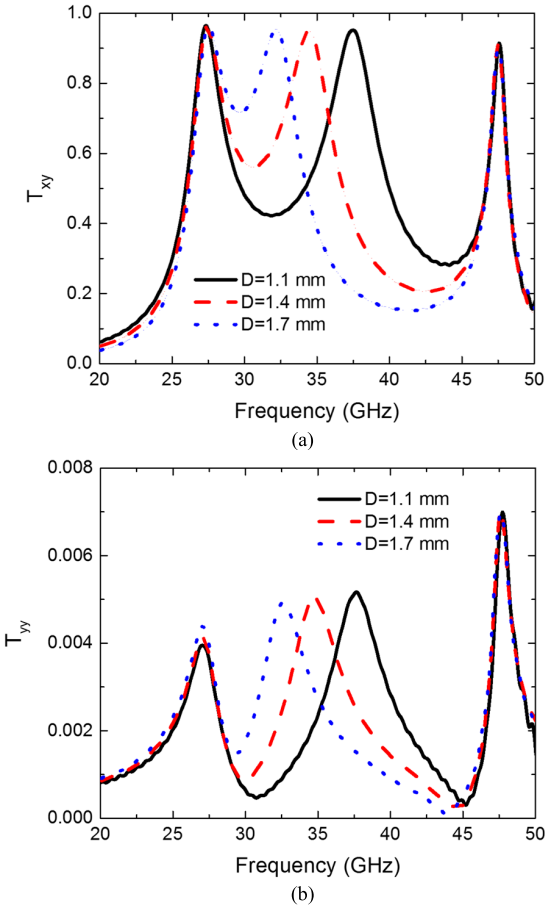

Fig. 5. Simulated transmission coefficients of the polarization converter as a function of D. (a) T_{xy} and (b) T_{yy}.

be moved close to the first resonance frequency, f_A, and the broadband characteristics can be achieved.

B. Double Slot

To increase the bandwidth, the slot width was first considered as a design parameter. In the equivalent circuit model, a slot can be represented by a parallel *LC* circuit. The increased slot width extends the bandwidth because a wider slot exhibits larger inductance. However, the co-polarized transmission coefficient level (T_{yy}) of the polarization converter also increases because the co-polarized transmission of the polarization converter is determined by the ratio of slot width over the slot length. Thus, there exists a tradeoff between the PCR and the bandwidth of the polarization converter. To achieve a low transmission coefficient level of T_{yy}, the slot width cannot be increased any further. Thus, two narrow slot apertures are used for bandwidth enhancement instead of a single wide slot.

When double narrow slots are used for a polarization converter, as shown in Fig. 6, broadband characteristics can be achieved without sacrificing PCR. With the double narrow slots, the resonance modes of the double slots are coupled, and their resonance characteristics are similar to that of a single wide slot. Thus, the cross-polarized transmission coefficient (T_{xy}) of the double narrow slots is similar to that of the single

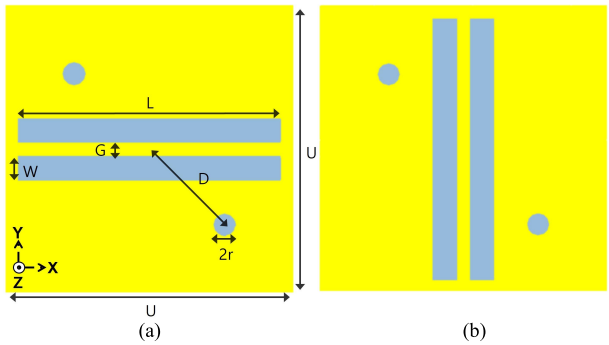

Fig. 6. Schematic design of unit cell of the polarization converter with double slots. (a) Front side and (b) back side. L = 4.2 mm, W = 0.4 mm, D = 1.4 mm, r = 0.2 mm, U = 4.6 mm, G = 0.1 mm, and the substrate thickness (T_S) = 0.8 mm.

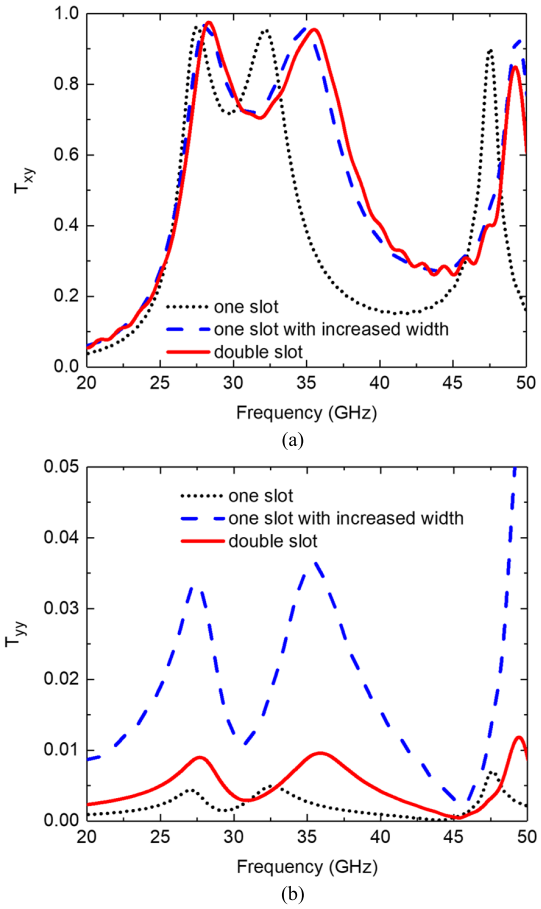

Fig. 7. Simulated transmission coefficients of the polarization converter based on two slots. (a) T_{xy} and (b) T_{yy}.

wide slot, and essentially, the same bandwidth enhancement can be achieved. However, the co-polarized transmission coefficient (T_{yy}) of the double narrow slots is much lower than that of a single wide slot, as shown in Fig. 7.

This design offers a new parameter, which is the distance between the two slots (G). When the distance is increased, f_A and f_C are blue-shifted, which makes the three resonance frequencies closer. This can be explained by surface charge and current distribution. The first resonance frequency, f_A, is affected by the surface current path length on the metal surface between neighboring unit cells. When double slots are

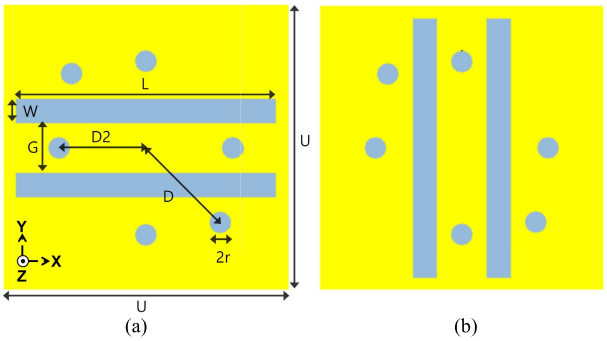

Fig. 8. Schematic design of unit cell of the polarization converter with four additional via holes. (a) Front side and (b) back side.

used and the distance between the two slots is increased, the opposite charges in the neighboring unit cells get closer. This results in shorter current path length and higher resonance frequency, f_A. The resonance frequency, f_B, is affected by the distance between the via hole and the slot. As the distance between the two slots (G) is increased, the distance between the slot and via hole is reduced. Thus, the second resonance frequency, f_B, increases. From these effects of two slots, three resonance frequencies get closer and the broad frequency band is achieved.

C. Additional via Holes at the Same Distance From Center

A subsequent polarization converter design is proposed in consideration of the charge distribution at each resonance frequency. To combine three resonance frequencies, four via holes were added to the previous design shown in Fig. 8.

Four via holes were located so as to change the surface charge and current distribution, which makes the three resonance frequencies closer to each other. Two via holes are located to the right and left areas of two slots on the back side and the other two via holes are located above and below the two slots on the front side to control their f_A and f_B. Because the front side acts as a receiver antenna and the back side acts as a transmitter antenna, the two sides must have the same resonance characteristics. At f_A, two via holes on the right and left sides push opposite charges into the corner, which makes f_A blue-shifted (as illustrated in Fig. 9). The two via holes also push the charges toward the slot at the second resonance frequency, which makes the current path length shorter. At f_C, most of the charges are distributed at the upper right and lower left corner of the unit cell, so that the additional via holes do not affect the charge distribution or resonance frequency. By placing additional via holes, f_A and f_B are blue-shifted, but f_C is almost invariant. It enables the three frequency bands to be combined and to exhibit broader bandwidth.

III. Fabrication and Measurement

The proposed polarization converter was fabricated on Teflon (TLX-9) with a relative permittivity of 2.5 and a dielectric loss tangent of 0.0017 at 30 GHz. The copper thickness was 18 μm. Via holes were drilled to connect the front side electrically with the back side. The size of the fabricated polarization converter consisting of 17 $\times$ 17 unit cells was 105 $\times$ 105 mm.

The fabricated polarization converter was characterized using two horn antennas. Two linearly polarized horn antennas were connected to a vector network analyzer. The distance between the two antennas was 1.4 m, and the fabricated samples were placed in the center between the two antennas. To minimize the edge-diffraction effect, an absorbing material (60 $\times$ 60 cm) was placed around each sample. The absorbing material had an absorbance higher than 40 dB in the frequency range from 20 to 50 GHz. A polarization mismatch was considered for accurate measurement of the co-polarized transmission. To get a low level of co-polarized transmission, the polarization of the transmitted wave and the orientation of the receiver antenna should be perpendicular. By using the jig shown in Fig. 10, the azimuth angle of each sample was adjusted to achieve a low level of co-polarized transmission. The simulated transmittance and PCRs of the presented polarization converter showed ultrawideband characteristics; so, three types of horn antennas (K-band horn antenna covering from 18.5 to 26.5 GHz, Ka-band horn antenna covering from 26.5 to 40 GHz, and Q-band horn antenna covering from 33 to 50 GHz) were used for measurement.

In Fig. 11, the comparisons of the simulated and measured transmittance results for each polarization converter design are shown. The geometric dimensions of Design 1 were as follows: L = 4.2 mm, W = 0.4 mm, D = 1.4 mm, r = 0.2 mm, and U = 4.6 mm. The measured and simulated transmittances of the y-to-x polarization conversion were almost identical. The measured 3 dB fractional bandwidth of transmittance of the y-to-x polarization conversion was 24.2%. The measured transmittance level of y-to-y polarization was higher than the simulated one, but this was because the cross-polarization polarization level of the utilized horn antenna was -38 dB.

When two slots are used for the polarization converter in Design 2, the transmittance response shows a broader bandwidth. The geometric dimensions are the same as those of Design 1 except the distance between two slots, which is 1.7 mm. The measured 3 dB fractional bandwidth at y-to-x polarization conversion was 31%. By using two slots, the maximum co-polarized transmittance level was increased to more than -30 dB.

In Design 3, as three resonance frequencies increase due to additional via holes, the unit cell size and slot length are increased to cover the Ka-band. The geometric dimensions were as follows: L = 5.6 mm, W = 0.4 mm, D = 1.75 mm, r = 0.2 mm, U = 6 mm, G = 1 mm, and D2 = 1.6 mm. The measured 3 dB fractional bandwidth at y-to-x polarization conversion was 40.4%. Because the additional via holes can only help to increase the fraction bandwidth at the y-to-x polarization conversion but maintain co-polarized the transmittance level, the co-polarized transmittance level still remains below -30 dB.

The PCR for the y-polarized incident wave is defined as $t_{xy}/(t_{xy} + t_{yy})$ by using the measured transmittance t_{xy} and t_{yy}. The operating frequency band, where the PCR is higher than 99%, is from 24.5 to 47 GHz, as shown in Fig. 12. This means nearly perfect 90° polarization rotation is achieved

TABLE I
COMPARISON OF THE STATE-OF-THE-ART POLARIZATION CONVERTERS

Reference	Type	Fractional Bandwidth (%) @ PCR ≥99%	Electrical thickness of unit cell	FoM
[19]	Reflection	14.5% (16~18.5 GHz)	0.193•λ_g	0.751
[27]	Reflection	25% (14~18 GHz)	0.502•λ_g	0.498
[28]	Reflection	40% (14~21 GHz)	0.549•λ_g	0.728
[11]	Transmission	19.1% (9.5~11.51 GHz)	0.088•λ_g	2.166
[13]	Transmission	9.5% (8~8.8 GHz)	0.068•λ_g	1.393
[24]	Transmission	11.9% (0.95~1.071 THz)	0.212•λ_g	0.566
[26]	Transmission	9.3% (33.6~36.9 GHz)	0.274•λ_g	0.342
This work	Transmission	62.9% (24.5~47 GHz)	0.151•λ_g	4.175

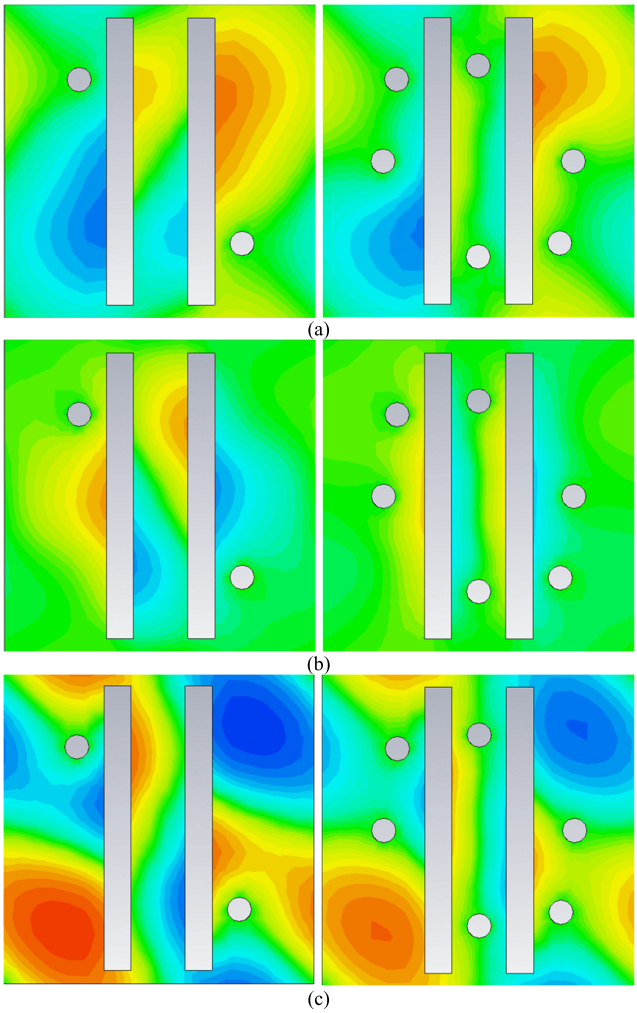

Fig. 9. Change of charge distributions on the back side of the polarization converter with and without additional via holes at the (a) first, (b) second, and (c) third resonance frequencies.

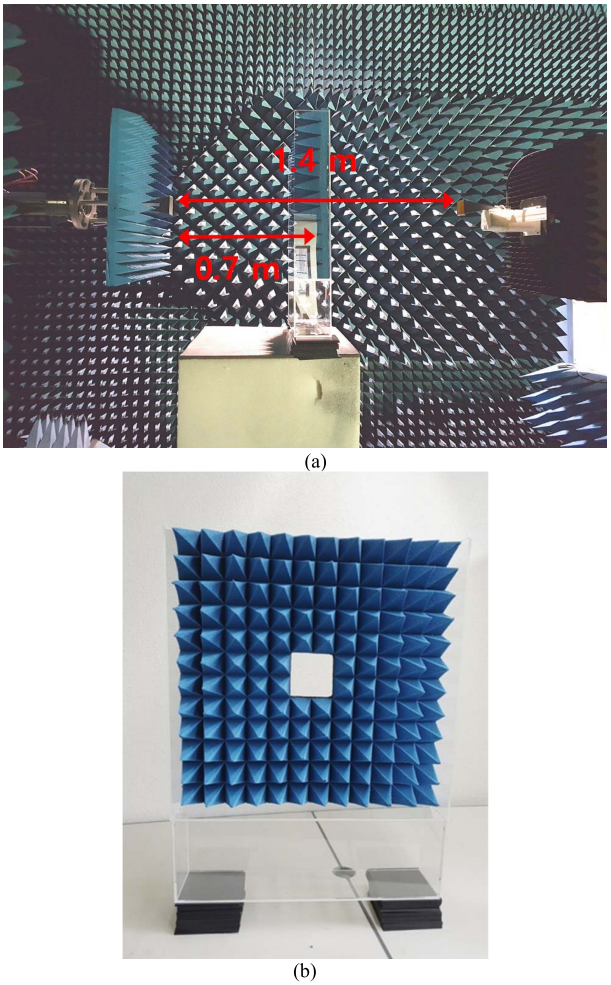

Fig. 10. (a) Measurement setup and (b) jig for control of azimuth angle.

in this frequency range. Even though it is not shown in this article, a simulation study showed that the PCR performance degraded for the electromagnetic wave incidence at an oblique angle [30].

The performance of the polarization converter in this work is compared with those of other linear-to-linear polarization converters in Table I. When the fractional bandwidth is defined for the frequency band where the PCR is higher than 90%, the reflection-type polarization converters in [27] and [28] exhibit the fractional bandwidth of 115%–122%. The reflection-type polarization converters with thick substrates exhibit much wider band characteristics than the transmission-type polarization converters do. For perfect polarization conversion, the PCR higher than 99% is required. Thus, the fractional bandwidth in Table I is defined, where the PCR is higher than 99%.

To compare the performance of the thin-film polarization converters, of which the operational frequency bands are different, the figure of merit (FoM) defined in (1) was utilized in [5] and [30]

$$\text{FoM} = \frac{\Delta\omega}{\omega_0} \cdot \frac{\lambda_g}{T_s} \tag{1}$$

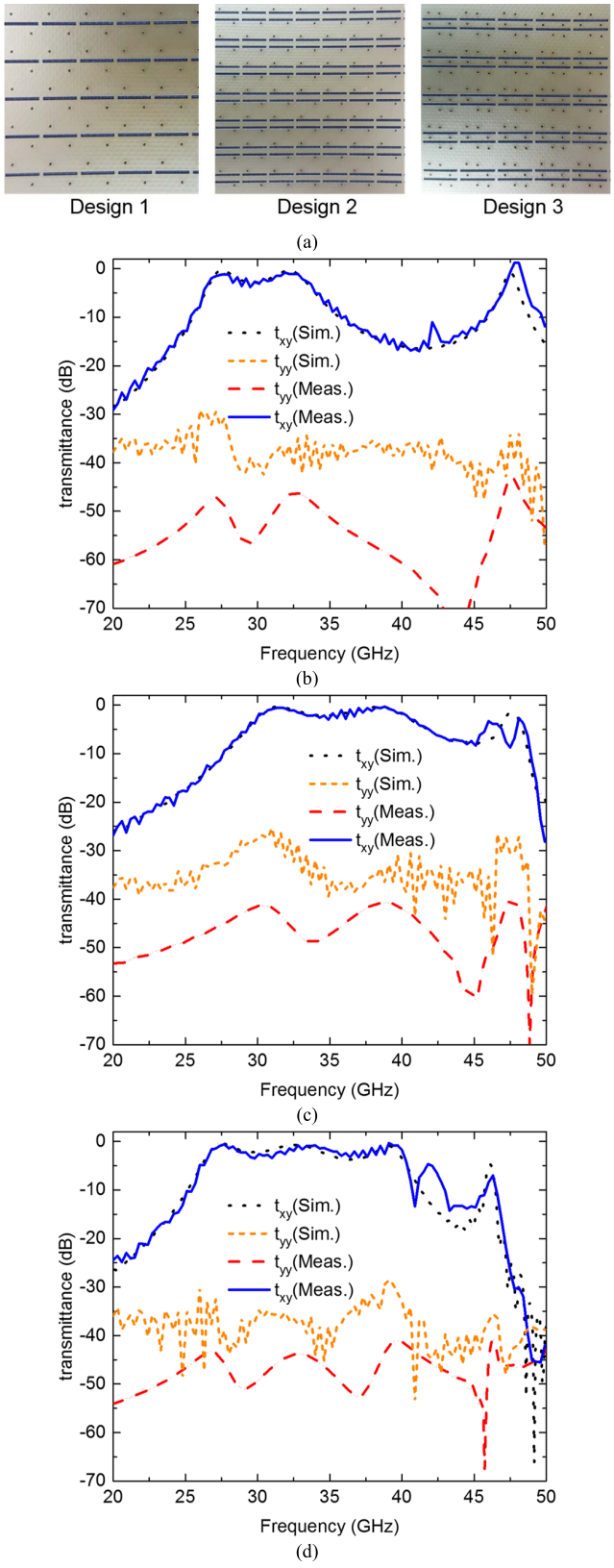

Fig. 11. Comparison of the simulated and measured transmittance of the polarization converter. (a) Sample images. (b) Design 1. (c) Design 2. (d) Design 3.

where $\Delta\omega/\omega_o$ is the fractional bandwidth, where PCR $\geq$ 99%, λ_g is the central wavelength of operating band, and T_s is the thickness of the device [5], [30], [31], [32]. The FoM shows how large bandwidth can be achieved with a given thickness of FSS or metasurface. For the same design, the bandwidth of the device increases when the thickness increases.

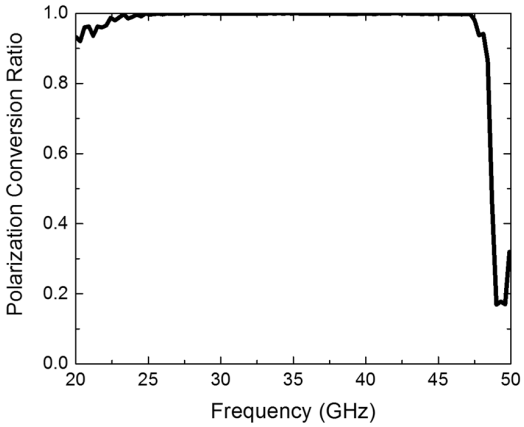

Fig. 12. PCR at Design 3.

The proposed converter exhibits much higher FoM than the other polarization converters as compared in Table I. This implies that the presented converter design can achieve very high PCR in ultrawide bandwidth even on the very thin substrate.

IV. Conclusion

A broadband linear-to-linear polarization converter was demonstrated by using a bilayer slot structure connected by via holes on a single PCB substrate. Because the front- and back-side slots orthogonal to each other and connecting via holes are combined, surface current occurs in various directions. This indicates that the slot length is not the only parameter determining resonance frequencies. The operational characteristics of the broadband polarization converters were investigated by considering the surface charge and current distribution. Proper positioning of the via holes around the slot apertures enabled control of broadband polarization conversion characteristics by combining multiple frequency bands. The proposed polarization converter exhibits perfect PCR ($\geq$99%) at frequencies ranging from 24.5 to 47 GHz (fractional bandwidth of 62.9%) and FoM of 4.175. This shows that the presented structures can realize much wider bandwidth than other reported designs, within the limited device volume.

References

[1] Y. Zheng et al., "Ultra-wideband polarization conversion metasurface and its application cases for antenna radiation enhancement and scattering suppression," *Sci. Rep.*, vol. 7, p. 16137, Nov. 2017.

[2] Y. Liu, K. Li, Y. Jia, Y. Hao, S. Gong, and Y. J. Guo, "Wideband RCS reduction of a slot array antenna using polarization conversion metasurfaces," *IEEE Trans. Antennas Propag.*, vol. 64, no. 1, pp. 326–331, Jan. 2016.

[3] W. Sun, Q. He, J. Hao, and L. Zhou, "A transparent metamaterial to manipulate electromagnetic wave polarizations," *Opt. Lett.*, vol. 36, no. 6, pp. 927–929, 2011.

[4] B. Gimeno, J. L. Cruz, E. A. Navarro, and V. Such, "A polarizer rotator system for three-dimensional oblique incidence," *IEEE Trans. Antennas Propag.*, vol. 42, no. 7, pp. 912–919, Jul. 1994.

[5] S. A. Winkler, W. Hong, M. Bozzi, and K. Wu, "Polarization rotating frequency selective surface based on substrate integrated waveguide technology," *IEEE Trans. Antennas Propag.*, vol. 58, no. 4, pp. 1202–1213, Apr. 2010.

[6] Y. Cheng, Y. Nie, X. Wang, and R. Gong, "An ultrathin transparent metamaterial polarization transformer based on a twist-split-ring resonator," *Appl. Phys. A, Solids Surf.*, vol. 111, no. 1, pp. 209–215, Apr. 2013.
[7] G. Zhou et al., "Designing perfect linear polarization converters using perfect electric and magnetic conducting surfaces," *Sci. Rep.*, vol. 6, p. 38925, Dec. 2016.
[8] T. Nose, S. Sato, K. Mizuno, J. Bae, and T. Nozokido, "Refractive index of nematic liquid crystals in the submillimeter wave region," *Appl. Opt.*, vol. 36, no. 25, pp. 6383–6387, 1997.
[9] C.-Y. Chen, T.-R. Tsai, C.-L. Pan, and R.-P. Pan, "Room temperature terahertz phase shifter based on magnetically controlled birefringence in liquid crystals," *Appl. Phys. Lett.*, vol. 83, no. 22, pp. 4497–4499, Dec. 2003.
[10] M. Mutlu and E. Ozbay, "A transparent 90° polarization rotator by combining chirality and electromagnetic wave tunneling," *Appl. Phys. Lett.*, vol. 100, no. 5, 2012, Art. no. 051909.
[11] Z. Wei, Y. Cao, Y. Fan, X. Yu, and H. Li, "Broadband polarization transformation via enhanced asymmetric transmission through arrays of twisted complementary split-ring resonators," *Appl. Phys. Lett.*, vol. 99, Nov. 2011, Art. no. 221907.
[12] H. Shi, A. Zhang, S. Zheng, J. Li, and Y. Jiang, "Dual-band polarization angle independent 90° polarization rotator using twisted electric-field-coupled resonators," *Appl. Phys. Lett.*, vol. 104, no. 3, 2014, Art. no. 034102.
[13] J. H. Shi, H. F. Ma, C. Y. Guan, Z. P. Wang, and T. J. Cui, "Broadband chirality and asymmetric transmission in ultrathin 90°-twisted Babinet-inverted metasurfaces," *Phys. Rev. B, Condens. Matter*, vol. 89, no. 16, 2014, Art. no. 165128.
[14] J. H. Shi, H. F. Ma, W. X. Jiang, and T. J. Cui, "Multiband stereometamaterial-based polarization spectral filter," *Phys. Rev. B, Condens. Matter*, vol. 86, no. 3, Jul. 2012, Art. no. 035103.
[15] N. K. Grady et al., "Terahertz metamaterials for linear polarization conversion and anomalous refraction," *Science*, vol. 340, no. 6138, pp. 1304–1307, 2013.
[16] W. Li et al., "Design of a dual-band dual-polarization transparent frequency selective surface," *IEEE Antennas Wireless Propag. Lett.*, vol. 16, pp. 3172–3175, 2017.
[17] Y. Cheng, R. Gong, and L. Wu, "Ultra-broadband linear polarization conversion via diode-like asymmetric transmission with composite metamaterial for terahertz waves," *Plasmonics*, vol. 12, no. 4, pp. 1113–1120, Aug. 2017.
[18] X. Wen and J. Zheng, "Broadband THz reflective polarization rotator by multiple plasmon resonances," *Opt. Exp.*, vol. 22, no. 23, pp. 28292–28300, Nov. 2014.
[19] X. Gao, X. Han, W.-P. Cao, H. O. Li, H. F. Ma, and T. J. Cui, "Ultrawideband and high-efficiency linear polarization converter based on double V-shaped metasurface," *IEEE Trans. Antennas Propag.*, vol. 63, no. 8, pp. 3522–3530, Aug. 2015.
[20] X. Liu et al., "An analytical design of cross polarization converter based on the gangbuster metasurface," *IEEE Antennas Wireless Propag. Lett.*, vol. 16, pp. 1028–1031, 2017.
[21] G. Zhou et al., "A broadband reflective-type half-wave plate employing optical feedbacks," *Sci. Rep.*, vol. 7, p. 9103, Aug. 2017.
[22] Q. Levesque et al., "Plasmonic planar antenna for wideband and efficient linear polarization conversion," *Appl. Phys. Lett.*, vol. 104, no. 11, 2014, Art. no. 111105.
[23] X.-C. Zhu et al., "A novel reflective surface with polarization rotation characteristic," *IEEE Antennas Wireless Propag. Lett.*, vol. 12, pp. 968–971, 2013.
[24] J. M. Woo, S. Hussain, and J.-H. Jang, "A terahertz in-line polarization converter based on through-via connected double layer slot structures," *Sci. Rep.*, vol. 7, no. 1, p. 42952, Mar. 2017.
[25] R. C. Johnson and H. Jasik, *Antenna Engineering Handbook*. New York, NY, USA: McGraw-Hill, 1984.
[26] X.-C. Zhu et al., "Design of a bandwidth-enhanced polarization rotating frequency selective surface," *IEEE Trans. Antennas Propag.*, vol. 62, no. 2, pp. 940–944, Feb. 2014.
[27] M. S. J. Moghadam, M. Akbari, F. Samadi, and A.-R. Sebak, "Wideband cross polarization rotation based on reflective anisotropic surfaces," *IEEE Access*, vol. 6, pp. 15919–15925, 2018.
[28] F. Samadi, M. Akbari, M. R. Chaharmir, and A. Sebak, "Scatterer surface design for wave scattering application," *IEEE Trans. Antenna Propag.*, vol. 67, no. 2, pp. 1202–1211, Feb. 2018.
[29] M. Akbari, F. Samadi, A.-R. Sebak, and T. A. Denidni, "Superbroadband diffuse wave scattering based on coding metasurfaces: Polarization conversion metasurfaces," *IEEE Antennas Propag. Mag.*, vol. 61, no. 2, pp. 40–52, Apr. 2019.
[30] P. Xu, W. X. Jiang, S. Y. Wang, and T. J. Cui, "An ultrathin cross-polarization converter with near unity efficiency for transmitted waves," *IEEE Trans. Antennas Propag.*, vol. 66, no. 8, pp. 4370–4373, Aug. 2018.
[31] T. Deng, Z.-W. Li, and Z. N. Chen, "Ultrathin broadband absorber using frequency-selective surface and frequency-dispersive magnetic materials," *IEEE Trans. Antennas Propag.*, vol. 65, no. 11, pp. 5886–5894, Nov. 2017.
[32] F. F. Li, Q. Lou, P. Chen, Y. Poo, and R. X. Wu, "Broadband backscattering reduction realized by array of lossy scatterers," *Opt. Exp.*, vol. 26, no. 26, pp. 34711–34718, 2018.
[33] C. K. Lee, W. X. Zhong, and S. Y. R. Hui, "Effects of magnetic coupling of nonadjacent resonators on wireless power domino-resonator systems," *IEEE Trans. Power Electron.*, vol. 27, no. 4, pp. 1905–1916, Apr. 2012.

Jun-Ho Jeong was born in Ulsan, South Korea, in 1991. He received the B.S. degree in electrical engineering from the University of Seoul, Seoul, South Korea, in 2016, and the M.S. degree in electrical engineering and computer science from the Gwangju Institute of Science and Technology (GIST), Gwangju, South Korea, in 2018.

He is currently a Process Engineer with the Memory Division, Samsung electronics, Hwasung, South Korea. His research interests include frequency selective surface-based electromagnetic relaying devices and metamaterial structures.

Jae-Yeong Lee (Member, IEEE) received the B.S. and M.S. degrees in wireless communications engineering from Kwangwoon University, Seoul, South Korea, in 2008 and 2010, respectively, and the Ph.D. degree from the Gwangju Institute of Science and Technology (GIST), Gwangju, South Korea, in 2018.

He worked as a Post-Doctoral Fellow and a Research Assistant Professor with the Department of Electrical Engineering, Pohang University of Science and Technology (POSTECH), Pohang, South Korea, until 2022. He is currently a Senior Researcher with the Terahertz Research Section, Electronics and Telecommunications Research Institute (ETRI), Daejeon, South Korea, in 2022. His research interests include solid-state electronic materials/packaging-based RF devices and systems, mm-Wave/sub-THz optoelectronic devices for imaging security systems, high power/voltage microwave/mm-Wave device module for electronic warfare applications, and electrically reconfigurable metamaterials-based microwave/mm-Wave/sub-THz antennas.

Jae-Hyung Jang (Senior Member, IEEE) received the B.S. and M.S. degrees in electrical engineering from Seoul National University, Seoul, South Korea, in 1993 and 1995, respectively, and the Ph.D. degree in electrical and computer engineering from the University of Illinois at Urbana–Champaign (UIUC), Urbana, IL, USA, in 2002.

He is currently a Professor and the Associate Dean of the Graduate School and the Chair of the School of Energy Engineering, Korea Institute of Energy Technology (KENTECH), Naju, South Korea. Before joining KENTECH in 2021, he has been a Professor in electrical engineering and computer science with the Gwangju Institute of Science and Technology (GIST), Gwangju, South Korea, since 2004. During his stay at GIST, he served as the Chair of Electrical Engineering and Computer Science from 2019 to 2021 and the Director of the Research Institute of Solar Energy (RISE) from 2015 to 2019. His research interests include InP optoelectronic devices, SiC and GaN-based electron devices, GaAs, and CIGS-based thin-film solar cells. He is also doing active research on active metamaterial devices for microwave and THz applications.

Dr. Jang is a Committee Member of IEEE Compound Semiconductor Devices and Circuit Division and a member of the Board of Directors at Korea Photovoltaics Society.